




Article

# Mg<sup>2+</sup> is a Missing Link in Plant Cell Ca<sup>2+</sup> Signalling and Homeostasis—A Study on *Vicia faba* Guard Cells

Fouad Lemtiri-Chlieh <sup>1,2,\*</sup>, Stefan T. Arold <sup>1,3,4</sup> and Chris Gehring <sup>1,5,\*</sup> 

<sup>1</sup> King Abdullah University of Science and Technology (KAUST), Biological and Environmental Science and Engineering (BESE), Thuwal 23955-6900, Saudi Arabia; stefan.arold@KAUST.edu.sa

<sup>2</sup> Department of Neuroscience, University of Connecticut School of Medicine, Farmington, CT 06030, USA

<sup>3</sup> King Abdullah University of Science and Technology (KAUST), Computational Bioscience Research Center (CBRC), Thuwal 23955-6900, Saudi Arabia

<sup>4</sup> Centre de Biochimie Structurale, CNRS, INSERM, Université de Montpellier, 34090 Montpellier, France

<sup>5</sup> Department of Chemistry, Biology & Biotechnology, University of Perugia, 06121 Perugia, Italy

\* Correspondence: FLemtiriChlieh@uchc.edu (F.L.-C.); christophandreas.gehring@UniPG.it (C.G.)

Received: 28 March 2020; Accepted: 15 May 2020; Published: 27 May 2020



**Abstract:** Hyperpolarization-activated calcium channels (HACCs) are found in the plasma membrane and tonoplast of many plant cell types, where they have an important role in Ca<sup>2+</sup>-dependent signalling. The unusual gating properties of HACCs in plants, i.e., activation by membrane hyperpolarization rather than depolarization, dictates that HACCs are normally open in the physiological hyperpolarized resting membrane potential state (the so-called pump or P-state); thus, if not regulated, they would continuously leak Ca<sup>2+</sup> into cells. HACCs are permeable to Ca<sup>2+</sup>, Ba<sup>2+</sup>, and Mg<sup>2+</sup>; activated by H<sub>2</sub>O<sub>2</sub> and the plant hormone abscisic acid (ABA); and their activity in guard cells is greatly reduced by increasing amounts of free cytosolic Ca<sup>2+</sup> ([Ca<sup>2+</sup>]<sub>Cyt</sub>), and hence closes during [Ca<sup>2+</sup>]<sub>Cyt</sub> surges. Here, we demonstrate that the presence of the commonly used Mg-ATP inside the guard cell greatly reduces HACC activity, especially at voltages ≤ −200 mV, and that Mg<sup>2+</sup> causes this block. Therefore, we firstly conclude that physiological cytosolic Mg<sup>2+</sup> levels affect HACC gating and that channel opening requires either high negative voltages (≥ −200 mV) or displacement of Mg<sup>2+</sup> away from the immediate vicinity of the channel. Secondly, based on structural comparisons with a Mg<sup>2+</sup>-sensitive animal inward-rectifying K<sup>+</sup> channel, we propose that the likely candidate HACCs described here are cyclic nucleotide gated channels (CNGCs), many of which also contain a conserved diacidic Mg<sup>2+</sup> binding motif within their pores. This conclusion is consistent with the electrophysiological data. Finally, we propose that Mg<sup>2+</sup>, much like in animal cells, is an important component in Ca<sup>2+</sup> signalling and homeostasis in plants.

**Keywords:** hyperpolarization-activated calcium channels; HACCs; cyclic nucleotides-activated channels; CNGCs; magnesium; calcium; guard cells; patch clamp; cellular homeostasis; structure modelling

## 1. Introduction

Ca<sup>2+</sup> has long been recognized as an essential component in many plant cellular processes. In order for Ca<sup>2+</sup> to function as an intracellular signal, temporal-, spatial-, and stimulus-specific changes in [Ca<sup>2+</sup>]<sub>Cyt</sub> need to be tightly controlled [1]. Ca<sup>2+</sup> influx into plant cells is achieved by three main types of Ca<sup>2+</sup> channels [2,3]: firstly, channels that show little or no voltage sensitivity, referred to as non-selective calcium channels (NSCCs), primarily for being active at all voltages and for being less selective for calcium over monovalent cations, such as K<sup>+</sup> and Na<sup>+</sup> [4]; secondly, channels that show high voltage-dependence, such as those activated by depolarization (DACCs) [5]; thirdly, others that are activated only by membrane hyperpolarization (HACCs) [6], which are the focus of this report.

In guard cells,  $\text{Ca}^{2+}$  was shown to be involved in abscisic acid (ABA) signalling and stomatal guard cell movements [7,8]. Using the patch clamp technique in both whole cell (WC) and excised configurations (EC), two types of HACCs were identified in the plasma membrane (PM). One type of HACCs is highly selective for  $\text{Ca}^{2+}$  (over  $\text{K}^+$  and  $\text{Cl}^-$ ) [9]. Its activity is enhanced by ABA [9,10],  $\text{H}_2\text{O}_2$  [10], and by external  $\text{Ca}^{2+}$  itself, an apparently unique property of this particular plant HACC [11]. Meanwhile, increasing  $[\text{Ca}^{2+}]_{\text{Cyt}}$  from 0.2 to 2  $\mu\text{M}$  decreased the open probability ( $P_o$ ) of this HACC by a factor of 10 [9], implying a critical role of  $[\text{Ca}^{2+}]_{\text{Cyt}}$  in the feedback regulation of the channel. The proteins responsible for this type of channel activity have not yet been identified. This is not the case for the other type of HACCs, where a family of 20 genes is known and their translation products were originally described as being mostly gated open by cyclic nucleotides, such as 3',5'-cyclic adenosine monophosphate (cAMP) or 3',5'-cyclic guanosine monophosphate (cGMP) [12]; hence, the reason for their name—cyclic nucleotide gated channels (CNGCs). Moreover, these plant channels, similarly to their animal functional homologs, poorly discriminate between divalent and monovalent cations. Indeed, when heterologously expressed in oocytes, these channels are not only permeable to  $\text{Ca}^{2+}$  [13] but are found to be equally permeable to monovalent cations such as  $\text{K}^+$ ,  $\text{Rb}^+$ ,  $\text{Na}^+$ ,  $\text{Li}^+$ , and  $\text{Cs}^+$  [13,14]. Similar inwardly rectifying currents ( $I$ ) permeable to either  $\text{Ca}^{2+}$ ,  $\text{Ba}^{2+}$ , and even  $\text{Na}^+$ , which are activated by cAMP [15] and cGMP [16], were also characterized in guard cells with the patch clamp technique. The latter work demonstrated that the highly expressed CNGC5 and CNGC6 genes in guard cells are directly responsible for the recorded HACC activity. Likewise, in pollen tubes of the Asian pear tree (*Pyrus pyrifolia* Nakai cv. Hosui), a HACC that conducts indiscriminately either  $\text{Ca}^{2+}$  or  $\text{K}^+$  was shown to be activated by cAMP and downregulated by high  $[\text{Ca}^{2+}]_{\text{Cyt}}$  [17]. It is noteworthy that all these HACCs share one common characteristic—they are sensitive to low concentrations of lanthanides [10,15–17].

We know from previous work, particularly in animal systems, that  $\text{Mg}^{2+}$  ions are key regulators of many ion channels and receptors [18]. For instance, the inwardly rectifying  $\text{K}^+$  ( $\text{K}_{\text{ir}}$ ) channels and TRPV6, a member belonging to a subgroup of transient receptor potential (TRP) cation channels, both show strong  $\text{Mg}^{2+}$ -dependent gating [19,20]. Another example of a voltage-dependent blockage by  $\text{Mg}^{2+}$  ions is the N-methyl-D-aspartate (NMDA) receptor [21,22]; in this case extracellular  $\text{Mg}^{2+}$  is responsible for this effect. By contrast, in plants, the rectification of  $I_{\text{K},\text{in}}$  was found not to be due to  $\text{Mg}^{2+}$ -dependent blockage [23] but rather due to an intrinsic property of the channel protein itself [24]. However, ion channels localized to the tonoplast with a key role in stomatal volume regulation, such as the slow (SV)- and the fast (FV)-activating vacuolar channels, were shown to be affected by cytosolic  $\text{Mg}^{2+}$  ions [25–28]. Indeed, it was found that besides  $\text{Ca}^{2+}$ ,  $\text{Mg}^{2+}$  also promoted the activation of SV channels, affecting their kinetics (time constants of channel activation and de-activation) and voltage-dependent activation characteristics. At the same time,  $\text{Mg}^{2+}$  inhibits FV channels, thus reducing  $\text{K}^+$  leakage from the tonoplast [25].  $\text{Mg}^{2+}$  was also shown to inhibit an outward NSCC, termed MgC, which was characterized in the PM of guard and subsidiary cells of *Vicia faba* and *Zea mays* [29]. Another NSCC example from  $\text{N}_2$ -fixing plants where  $\text{Mg}^{2+}$  plays a critical role is its involvement in the transport of ammonium ( $\text{NH}_4^+$ ) or ammonia ( $\text{NH}_3$ ) across the peribacteroid membrane [30]. This is partly achieved through a passive non-selective electrogenic transport system regulated by  $\text{Ca}^{2+}$ . More recently, this channel was described as having “unusual” characteristics, such as an inward rectification caused by  $\text{Mg}^{2+}$  on the cytosolic face and a very low single channel conductance (<0.2 pS with 150 mM KCl + 10 mM  $\text{CaCl}_2$  in the pipette and 150 mM  $\text{NH}_4^+$  in the bath), which was found to be inhibited by  $\text{Mg}^{2+}$  from the luminal face of the symbiosome [31].

ATP is another major regulator of ion channel gating. One of the best-characterized channels is  $\text{K}_{\text{ATP}}$ , an inward  $\text{K}^+$ -rectifier (from the  $\text{K}_{\text{ir}}$  family of genes) found mostly in cardiac and skeletal muscles, neurons, and pancreatic cells [18]. These channels are normally closed in the presence of ATP and only open to hyperpolarize the cell membrane when cytosolic ATP levels drop. ADP added in the form of Mg-ADP can restore the activity of  $\text{K}_{\text{ATP}}$  pre-treated with ATP [32,33]. In guard cells, Mg-ATP is required for blue light-activated outward currents [34]. Indeed, it was found that 1 to 2 mM Mg-ATP,

as well as other intracellular substrates, are required to fully activate a plasma membrane electrogenic ion pump capable of hyperpolarizing the membrane to around  $-140$  mV, a potential well beyond the activation threshold for  $I_{K,in}$  [35].

Given the importance of calcium channels in plant cellular signalling, including in guard cell aperture regulation, we address the question of whether internal  $Mg^{2+}$  can affect the activity HACCs in guard cell protoplasts (GCPs) and show examples of  $Gd^{3+}$ -sensitive  $Ba^{2+}$  currents ( $I_{Ba}$ ) activated by hyperpolarization with and without  $Mg^{2+}$  in the patch pipet. We also assess important properties of  $I_{Ba}$  in the absence of  $Mg^{2+}$ , such as the permeability and sensitivity to some relevant inorganic compounds and physiological effectors, including abscisic acid (ABA) and cAMP.

## 2. Materials and Methods

### 2.1. Protoplast Isolation

*Vicia faba* L. cv (Bunyan) Bunyan Exhibition seeds were grown on vermiculite under conditions described previously [36]. *Arabidopsis thaliana* (Columbia) seeds were grown on peat pellets (jiffy, Oslo) in a controlled environment growth chamber (Percival, CLF plant climatic, Wertenigen) at  $22$  °C on a 8/16-h light/dark cycle. Guard cell protoplasts (GCPs) were isolated from either week 3 or 4 in *V. faba* or from week 5 or 6 in *Arabidopsis thaliana* plants. GCPs were isolated from abaxial epidermal strips as described previously [37]. Briefly, epidermal strips were floated on medium containing 1.8–2.5% (*w/v*) Cellulase Onozuka RS (Yacult Honsha, Tokyo, Japan), 1.7–2% (*w/v*) Cellulysin (Calbiochem, Behring Diagnostics, La Jolla, CA, USA), 0.026% (*w/v*) Pectolyase Y-23, 0.26% (*w/v*) BSA, and 1 mM  $CaCl_2$  (pH 5.6), osmolality adjusted with sorbitol to  $360$  mOsm.kg<sup>-1</sup>. After 90–120 min incubation in the dark at  $28$  °C with gentle shaking, released protoplasts were passed through a  $30$  µm mesh and kept on ice for 2 to 3 min before centrifugation (100 g for 4 min at room temperature). The pellet consisting of GCPs was re-suspended and kept on ice in 1 or 2 mL of fresh medium containing 0.42 M mannitol, 10 mM 2-(N-morpholino) ethanesulfonic acid (Mes), 200 µM  $CaCl_2$ , 2.5 mM KOH (pH 5.55 and osmolality at  $466$  mOsm.kg<sup>-1</sup>). Unless stated otherwise, all chemicals were from Sigma (Sigma-Aldrich Co., St Louis, MO, USA).

### 2.2. Solutions

Protoplasts were placed in a 0.5 mL chamber, left to settle down, and then perfused continuously at a flow rate of  $\approx 0.5$ –1 mL/min. To record  $I_{Ba}$  currents through HACC, we used barium-containing solutions. The bath medium contained (in mM): 100  $BaCl_2$ , 10 Mes (pH 5.5 with Tris base); the pipette contained (in mM): 100  $BaCl_2$ , 4 EGTA, 10 Hepes (pH 7.5 with Tris). For experiments where  $I_{K,in}$  and  $I_{Ba}$  measurements were made on the same GCPs, a different bath and internal solutions as follows. Bath (in mM): 30 KCl, 10 Mes (pH 5.5 with Tris base) to measure  $I_{K,in}$ , which was replaced by 100  $BaCl_2$ , 10 Mes (pH 5.5 with Tris base) to measure  $I_{Ba}$ . Internal solution (in mM): 1  $BaCl_2$ , 18 KCl, 4 EGTA, 10 Hepes (pH 7.5 with Tris base). Mg-ATP,  $MgCl_2$ , or  $K_2$ -ATP were added as specified in the figures. Osmolality was adjusted with sorbitol to  $310$  mOsm.kg<sup>-1</sup>. For classic solutions used to measure  $I_{K,in}$  refer to [38]. ABA was added externally. All chemicals were from Sigma Chemical, Poole, Dorset, UK. The membrane permeable cAMP analog Bt<sub>2</sub>cAMP was solubilized in deionized water and stored in aliquots of 50–100 µL at a concentration of 0.1 M. Bt<sub>2</sub>cAMP was diluted to the final desired concentration just a few minutes before its use.

### 2.3. Current–Voltage Recording and Analysis

Patch pipettes (5–10) were pulled from Kimax-51 glass capillaries (Kimble 34500; Kimble, Owens-Illinois) using a two-stage puller (Narishige PP-83, Japan). Experiments were performed at room temperature ( $20$  to  $22$  °C) using standard whole-cell patch clamp techniques, with an Axopatch 200B integrating patch clamp amplifier (Axon Instruments, Inc., Union City, CA, USA). Voltage commands and simultaneous signal recordings and analyses were assessed by a microcomputer

connected to the amplifier via a multipurpose input–output device (Digidata 1320A) using pClamp software (versions 8.0 and 10; Axon Instruments, Inc.). After giga ohm seals were formed, the whole-cell configuration was then achieved by gentle suction and the membrane was immediately clamped to a holding voltage ( $h_V$ ) of  $-36$  mV. GCPs were continuously perfused throughout the experiment and current recordings began only after at least 5–10 min from going into whole-cell mode to allow for intracellular equilibrium between the cytoplasm and patch pipet solution. All current traces shown were low-pass filtered at 2 kHz before analog-to-digital conversion and were uncorrected for leakage current or capacitive transients. Membrane potentials were corrected for liquid junction potential as described in [39]. Ionic activities were calculated using GEOCHEM-EZ [40]. Current–voltage (I-V) relationships for  $I_{Ba}$  and  $I_{K,in}$  were plotted as steady-state currents vs. test potentials when using the square pulse stimulations or utilizing the “trace vs. trace” feature of Clampfit analysis when using voltage ramps. Unless otherwise stated, every experiment reported here was repeated a minimum of three times and data were graphed as mean  $\pm$  SEM.

#### 2.4. Protein Structural Modelling

Models were built using Swiss-Model [41] and structures were visualized with PyMOL (PyMOL Molecular Graphics System, Version 1.5.0.4 Schrödinger, LLC). Homology modelling was supported by PSIPRED [42] and multisequence alignments were produced with MUSCLE [43]. Alignments and additional information of the models are provided in the respective legends.

### 3. Results

#### 3.1. Removal of Intracellular Mg-ATP Unveils a Larger Instantaneously-Activated, Inwardly-Directed, and $Gd^{3+}$ -Sensitive $Ba^{2+}$ Current

We recorded  $Ba^{2+}$  currents ( $I_{Ba}$ ) in guard cell protoplasts in either the presence or absence of Mg-ATP (Figure 1A). At the end of the trials we also tested for  $I_{Ba}$  sensitivity to  $Gd^{3+}$ , a potent blocker of  $I_{Ba}$  (Figure 1B). The recorded currents were generated in response to a square pulse protocol from  $+64$  mV to  $-256$  mV in increments of  $-20$  mV, with the holding voltage ( $h_V$ ) set to  $-36$  mV. In the presence of Mg-ATP (Figure 1A; left panel), a small instantaneous inward-rectifying current of  $\approx -20$  pA started to activate at around  $-200$  mV, reaching a maximum of  $-60$  pA at  $-256$  mV. As expected, this current was sensitive to the addition of extracellular  $Gd^{3+}$  (see Figure 1B; left panel). Meanwhile, in the absence of Mg-ATP (Figure 1A; right panel), much larger ( $\geq 8$ -fold) instantaneous rectifying currents were recorded, which happened to also be  $Gd^{3+}$ -sensitive (Figure 1B; left traces). The current–voltage (I-V) relationships in the presence ( $\bullet$ ;  $n = 3$ ) or absence ( $\circ$ ;  $n = 7$ ) of Mg-ATP are represented in Figure 1C (left panel). We also plotted the effect of  $Gd^{3+}$  on the I-V relationships in the presence ( $\blacksquare$ ) or absence ( $\square$ ) of Mg-ATP (Figure 1C; right panel).

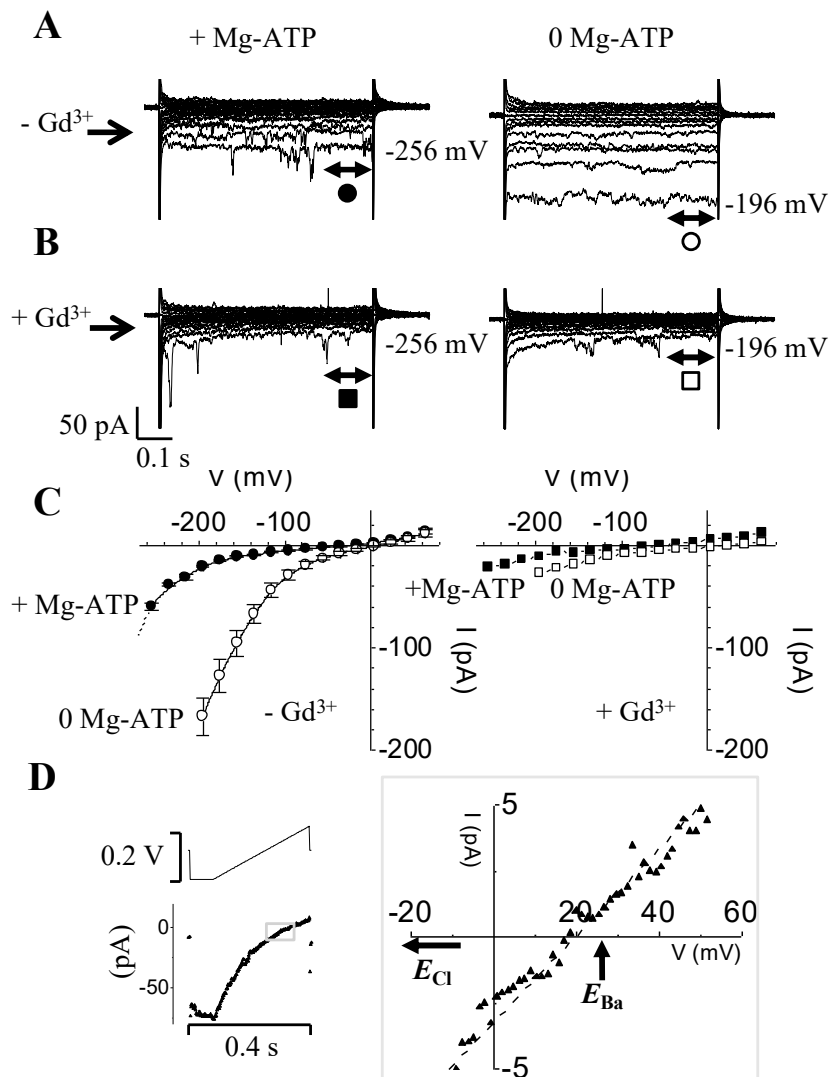


**Figure 1.** Removal of intracellular Mg-ATP unveils a larger instantaneously-activated, inwardly-directed, and Gd<sup>3+</sup>-sensitive Ba<sup>2+</sup> current. (A) Typical examples of current traces in whole-cell mode obtained from two separate *V. faba* guard cells with the pipette solution either containing (left traces) or lacking (right traces) Mg-ATP (1 mM). The pulse protocol mostly used throughout this study consisted of 0.6 s long square voltage pulses ranging from +64 to -256 mV in -20 mV increments; the holding potential  $h_v$  was set to -36 mV. In order to preserve the quality of the “giga” seals, guard cell protoplasts (GCPs) with no Mg-ATP in the pipette were not subjected to higher voltages beyond -196 mV. (B) Current ( $I$ ) traces of  $I_{Ba}$  obtained from the same cells and in the same conditions as described in (A), except for the external solution containing Gd<sup>3+</sup> (20 mM, left; or 100 mM, right) (C) Current–voltage relationships (I-V): left panel, superimposed I-Vs of  $I_{Ba}$  in the absence (○;  $n = 7$ ) or presence (●;  $n = 3$ ) of Mg-ATP; right panel, I-V relations in the presence of Gd<sup>3+</sup> (■: +Mg-ATP; □: -Mg-ATP). (D) The reversal potential ( $E_{rev}$ ) is close to the reversal potential for Ba<sup>2+</sup> ( $E_{Ba}$ ). Typical current trace recorded in the absence of Mg-ATP (below) in response to a voltage ramp which consists of activating  $I_{Ba}$  using a hyperpolarization square pulse to -156 mV and immediately followed by a continuous depolarizing ramp to +64 mV (the voltage protocol is depicted above), with a slope of  $0.7 \text{ V s}^{-1}$ . Scale bars are shown below the current traces and to the left of the voltage protocol.

These results highlight that when omitting Mg-ATP from the intracellular medium, a larger Gd<sup>3+</sup>-sensitive, inwardly rectifying Ba<sup>2+</sup> current is unveiled, which activates at significantly less-negative voltages (see the shift to the right of  $\geq -100$  mV in the I-V plot). Furthermore, the currents recorded in 0 Mg-ATP seem to reverse near the calculated Nernst equilibrium potential for

$\text{Ba}^{2+}$  ( $E_{\text{Ba}} \approx +28$  mV), and are far removed from  $E_{\text{Cl}}$  ( $-54$  mV). Likewise, using fast depolarization ramps ( $0.07$  V/s) after activating the current  $I_{\text{Ba}}$  with a square pulse to  $-156$  mV (see voltage protocol and current trajectories in Figure 1D; left), a reversal potential of  $+17$  mV was measured, again close to  $E_{\text{Ba}}$  rather than  $E_{\text{Cl}}$  (see Figure 1D, zoomed I-V plot). This is also indicative of the higher permeability of this conductance to  $\text{Ba}^{2+}$  as compared to  $\text{Cl}^-$ .

To test whether changing external  $\text{Ba}^{2+}$  concentration will affect current magnitude, as well as the I-V relationship, GCPs were patched in whole cell mode using the Mg-ATP-free internal solution (Figure 2).

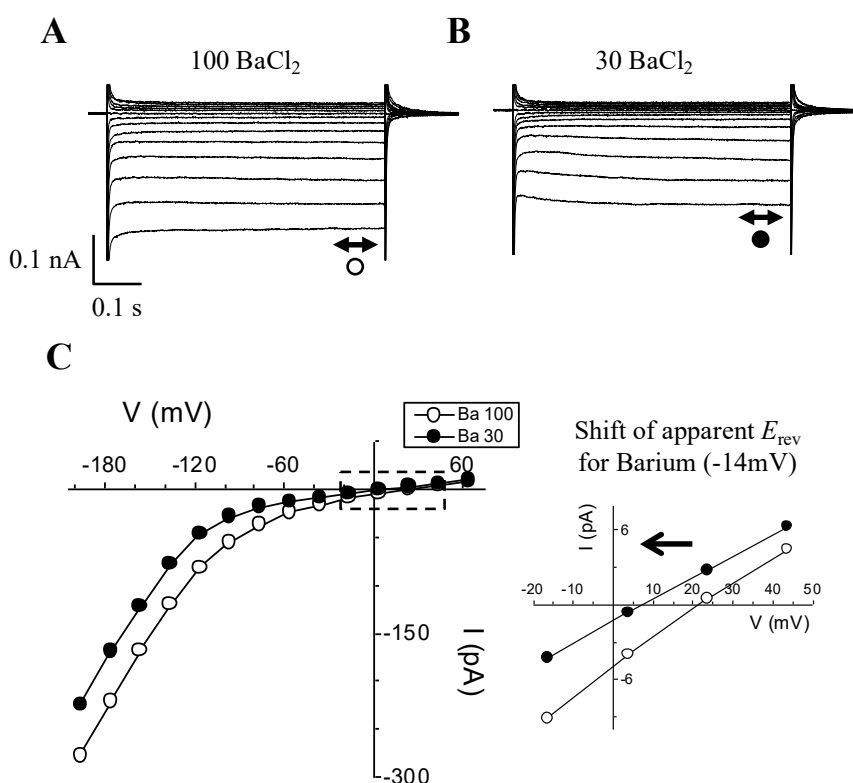


**Figure 2.** Decreasing  $[\text{Ba}^{2+}]_o$  from 100 to 30 mM not only decreases the hyperpolarization-activated  $I_{\text{Ba}}$  but also shifts its apparent reversal potential ( $E_{\text{rev}}$ ) ( $\sim -14$  mV). (A,B) Typical current traces of hyperpolarization-activated  $I_{\text{Ba}}$  recorded from the same *V. faba* guard cell in either 100 (A) or 30 mM (B)  $[\text{Ba}^{2+}]_o$ . Scale bars are shown below the current traces. (C) Corresponding I-V plots of  $I_{\text{Ba}}$  in 100 and 30 mM  $[\text{Ba}^{2+}]_o$  taken from the current traces shown in (A) and (B). Inset: Magnified I-V plot from the area shown as a dashed box in (C). The inset shows the amount (in mV) and the direction (arrow) of the shift in the apparent  $E_{\text{rev}}$  when the bath perfusion was switched from 100 to 30 mM  $\text{Ba}^{2+}$ .

Once again, the current magnitudes recorded in the absence of Mg-ATP are substantial. For instance, at  $-196$  mV, a  $-280$  pA current is measured in 100 mM  $[\text{Ba}^{2+}]_{\text{out}}$  (Figure 2A), while in 30 mM  $[\text{Ba}^{2+}]_{\text{out}}$  (Figure 2B) the same voltage gives rise to a current value of  $-220$  pA. All current magnitudes at any given voltage are decreased when switching to lower  $[\text{Ba}^{2+}]$  in the bath. The corresponding I-V plots appear as shifting to negative values (Figure 2C) when switching from 100 to 30 mM  $\text{Ba}^{2+}$ , which is accompanied by a negative shift in the apparent reversal potential ( $E_{\text{rev}}$ ) values. Indeed, when zooming in (Figure 2C, inset), the apparent  $E_{\text{rev}}$  shows a negative shift of  $\approx -14$  mV as a result of this  $\text{Ba}^{2+}$  concentration change. Furthermore, the apparent  $E_{\text{rev}}$  in 30 mM  $[\text{Ba}^{2+}]_{\text{out}}$  ( $\approx +8$  mV) is still closer to the calculated  $E_{\text{Ba}}$  rather than  $E_{\text{Cl}}$ , the values for which in this case are  $+17.7$  and  $-25.7$  mV, respectively. This experiment was repeated with 100, 30, and 10 mM  $\text{BaCl}_2$  in the bath, with the same qualitative effects observed, i.e., decrease of current amplitude when decreasing the  $[\text{Ba}^{2+}]_o$  and negative shift in the apparent  $E_{\text{rev}}$ .

### 3.2. HACC Permeability Sequence for Divalent Cations in the Absence of Mg-ATP: Ba > Ca ≈ Sr ≈ Mn >> Mg

Guard cell permeability to other divalent cations such as Ca<sup>2+</sup>, Sr<sup>2+</sup>, Mn<sup>2+</sup>, and Mg<sup>2+</sup> in the absence of Mg-ATP was also tested (Figure 3).

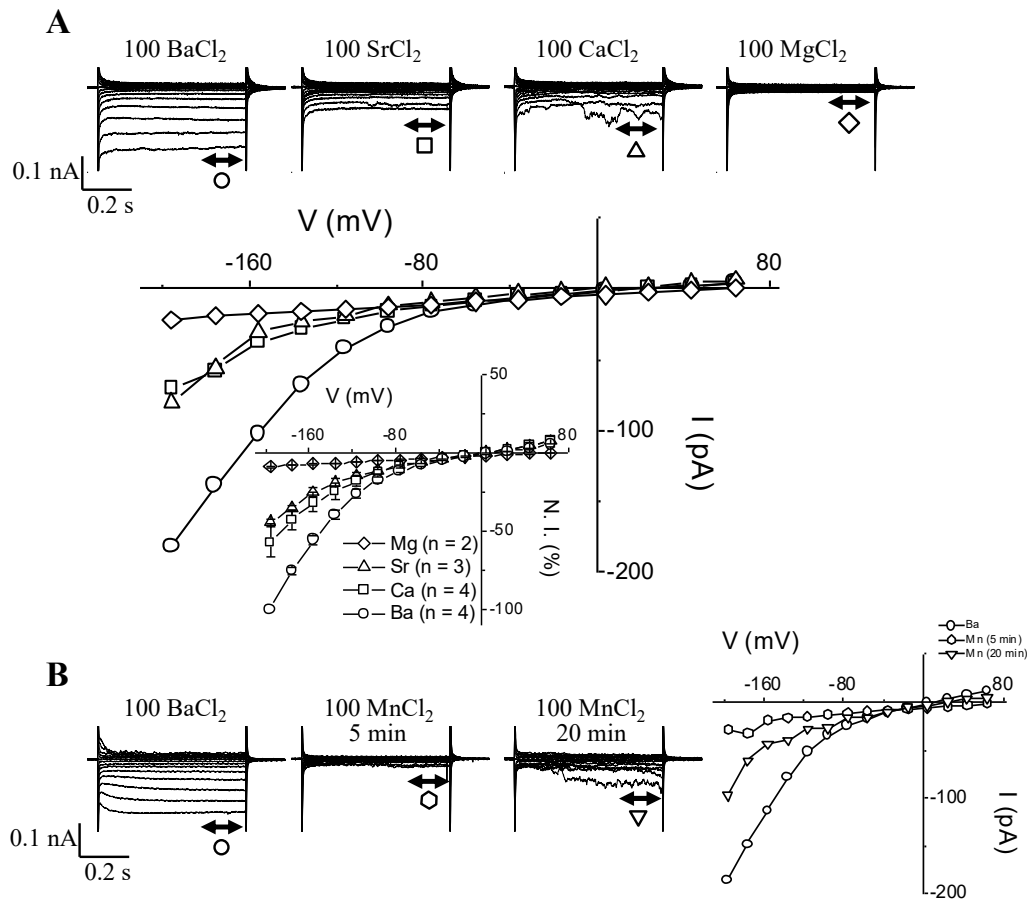


**Figure 3.** Current through  $I_{Ba}$  channels can be carried by other divalent cations, such as Ca<sup>2+</sup>, Sr<sup>2+</sup>, and even Mn<sup>2+</sup>, but not by Mg<sup>2+</sup>. (A) Typical current traces and corresponding I-V plots recorded in the presence of 100 mM BaCl<sub>2</sub>, 100 mM CaCl<sub>2</sub>, 100 mM SrCl<sub>2</sub>, and 100 mM MgCl<sub>2</sub> (note that all traces are from the same guard cell except for MgCl<sub>2</sub>). Inset: Normalized group I-V curves showing divalent permeabilities (the mean current values obtained for Ca<sup>2+</sup>, Sr<sup>2+</sup>, and Mg<sup>2+</sup> were normalized to the mean current value obtained in Ba<sup>2+</sup> at −196 mV). (B) Typical current traces and corresponding I-V plots recorded in the presence of 100 mM BaCl<sub>2</sub> and 100 mM MnCl<sub>2</sub> at 5 and 20 min. All traces are from the same guard cell. Notice the transient blocking effect of Mn<sup>2+</sup> ions.

As expected, HACC was permeable to Ca<sup>2+</sup> (Figure 3A) and found to have similar permeability to both Sr<sup>2+</sup> (Figure 3A) and Mn<sup>2+</sup> (Figure 3B). Meanwhile, Mg<sup>2+</sup> did not permeate HACC (Figure 3A). The I-V plots (Figure 3A,B) summarize the permeability data, i.e., the lack of HACC permeability to Mg<sup>2+</sup>, as well as the much larger permeability to Ba<sup>2+</sup> when compared to either Ca<sup>2+</sup>, Sr<sup>2+</sup>, or Mn<sup>2+</sup>. The effect of Mn<sup>2+</sup> ions over time is reported in Figure 3B and highlights the unique behavior of this ion. Unlike Ca<sup>2+</sup> or Sr<sup>2+</sup>, Mn<sup>2+</sup> (Figure 3B) triggered a transient blockage of HACC followed by some current recovery, while still washing out the Ba<sup>2+</sup> and replacing it with 100 mM Mn<sup>2+</sup>. This transient blockage effect was repeated on two other guard cell protoplasts but was never seen with either Ca<sup>2+</sup> or Sr<sup>2+</sup>, nor was it seen with Mg<sup>2+</sup>, even after 20 min of washing out the Ba<sup>2+</sup>.

### 3.3. HACC Permeability Sequence for Monovalent Cations in the Absence of Mg-ATP: $K \approx Na > Ba > Cs \gg TEA$

We observed that this  $Gd^{3+}$ -sensitive HACC is also permeable to some physiologically relevant monovalent cations, such as  $K^+$  (Figure S1A),  $Na^+$  (Figure S1B), and  $Cs^+$  (Figure S1C), but not tetraethylammonium ( $TEA^+$ ) (Figure S1D). These data indicate that the  $Gd^{3+}$ -sensitive current characterized in this work does not select for small mono or divalent cations (except for the case of  $Mg^{2+}$  and the bigger cation  $TEA^+$ ). Chloride also does not seem to permeate through this HACC. Indeed, when 100 mM  $Cl^-$  was added at the same time as  $TEA^+$  (see Figure S1D), no current could be detected, indicating that  $Cl^-$  is as impermeable as  $TEA^+$ . Qualitatively, the same effect was seen in all patched GCPs ( $n = 5$  for  $K^+$  and  $Na^+$ ;  $n = 2$  for  $Cs^+$  and  $TEA^+$ ).

### 3.4. Effect of Blockers of $I_{Ba}$ in the Absence of Mg-ATP and Comparison with the Effect on $I_{K,in}$

In order to further characterize this HACC, which was readily unmasked when Mg-ATP was omitted from the patch pipet, the effect of some classical blockers such as the lanthanides ( $La^{3+}$  and  $Gd^{3+}$ ),  $Mn^{2+}$ ,  $Cs^+$ , and  $TEA^+$  were tested on  $I_{Ba}$ , as well as on  $I_{K,in}$ , (the other major conductance that activates upon hyperpolarization in guard cells) (Figure 4).

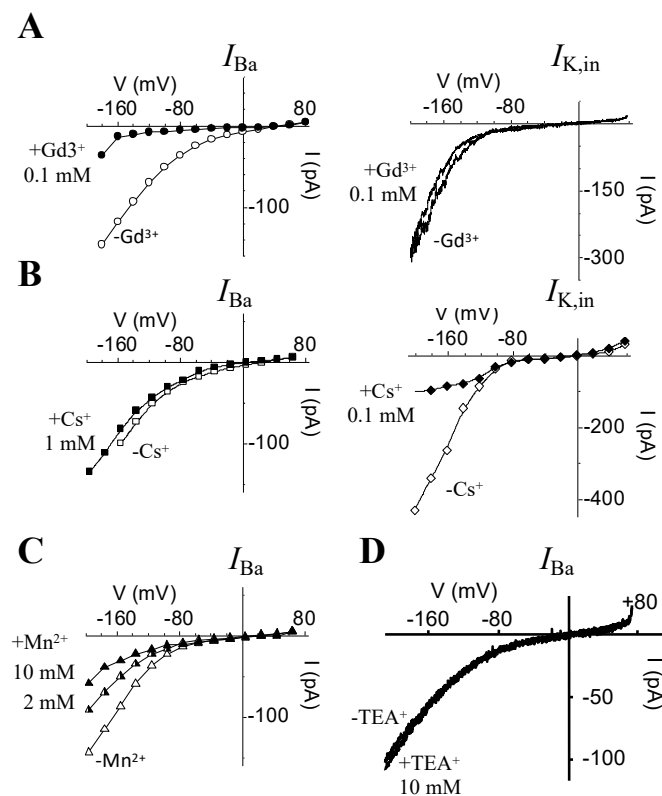


**Figure 4.** Differential effects of some known blockers on the two main PM conductances activated by hyperpolarization in guard cells, namely  $I_{Ba}$  and  $I_{K,in}$ . (A) I-V plots showing the effect of  $Gd^{3+}$  (0.1 mM) on  $I_{Ba}$  (left panel) and  $I_{K,in}$  (right panel). (B) I-V plots showing the effect of 1 mM  $Cs^+$  on  $I_{Ba}$  (left panel) compared to the effect of 0.1 mM  $Cs^+$  on  $I_{K,in}$  (right panel). (C) I-V plot showing the effect of  $Mn^{2+}$  on  $I_{Ba}$  recorded from the same GCP using 2 and 10 mM in the bath. (D)  $I_{Ba}$ -V plots generated from current recordings using hyperpolarizing ramps (+64 to  $-196$  mV;  $0.7$  V.s $^{-1}$ ;  $h_v = -36$  mV), showing the effect of 10 mM  $TEA^+$  added to the bath.

One of the most conspicuous effects lies in the potent effect of  $Gd^{3+}$  in blocking  $I_{Ba}$  (Figure 4A), even when used at relatively low concentrations (20 to 100  $\mu$ M), while the same concentrations of  $Gd^{3+}$  had no effect on  $I_{K,in}$  (Figure 4A). An even higher concentration of  $Gd^{3+}$  (500  $\mu$ M) did not affect



$I_{K,in}$  (data not shown).  $La^{3+}$  also blocked  $I_{Ba}$  measured in 0 Mg-ATP, but we found that much higher concentrations of  $La^{3+}$  (0.2 to 0.5 mM) are needed to achieve the same block as compared to  $Gd^{3+}$  (data not shown). Experimenting with cesium, a blocker of  $I_{K,in}$ , hardly any effect on  $I_{Ba}$  was registered (Figure 4B). Even though  $Cs^+$  was used at concentrations up to 1 mM, it had no or only a small effect on  $I_{Ba}$ , while one-tenth of this amount (0.1 mM) is sufficient to block a large proportion ( $\approx 80\%$  or more) of  $I_{K,in}$  (Figure 4B). Furthermore,  $Mn^{2+}$  used at 2 mM inhibited HACC by  $\approx 37\%$  (at  $V = -196$  mV) when the charge carrier (in this case  $Ba^{2+}$ ) was still present in the bath (Figure 4C). Increasing  $Mn^{2+}$  concentration to 10 mM shows that  $Mn^{2+}$  is not an efficient blocker of  $I_{Ba}$  as compared to  $Gd^{3+}$  or  $La^{3+}$ , and 10 mM  $Mn^{2+}$  only causes an extra 20%  $I_{Ba}$  inhibition (see IV plot in Figure 4C). Finally, 10 mM tetraethylammonium chloride (TEA), a concentration that was shown to block 70% to 80% of  $I_{K,in}$  in intact guard cells [44], had no effect whatsoever on  $I_{Ba}$  (Figure 4D) measured in 0 Mg-ATP.

### 3.5. Rapid Enhancement of $I_{Ba}$ by ABA

Given that in *V. faba* guard cells a HACC was implicated downstream of ABA in stomatal movements, we tested whether ABA affects  $I_{Ba}$  activated in the absence of internal Mg-ATP. We patch-clamped guard cells to measure  $I_{Ba}$  currents under baseline conditions, i.e., zero Mg-ATP inside and no added ABA outside (Figure 5).

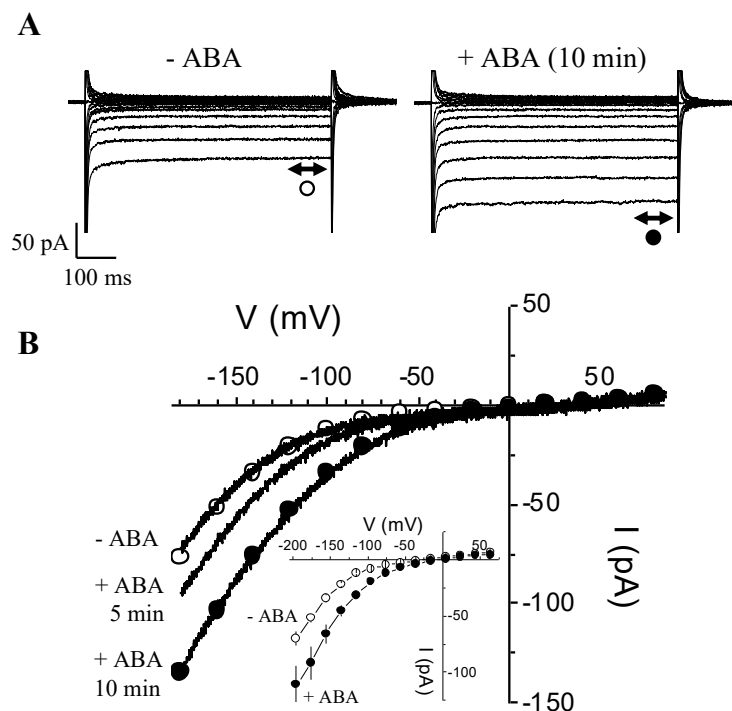


**Figure 5.** Rapid enhancement of  $I_{Ba}$  by abscisic acid (ABA). (A) The  $I_{Ba}$  currents in the absence of Mg-ATP in the patch pipet recorded from the same guard cell in response to hyperpolarizing voltages (from +64 to  $-196$  mV; in  $-20$  mV increments) before ( $\circ$ ) and 10 min after ( $\bullet$ ) bath application of ABA ( $20 \mu\text{M}$ ). (B) I-V plots of the effect of ABA, showing the enhancing effect of ABA with time (control: -ABA; 5 and 10 min after continuous bath perfusion with ABA). We also superimposed the measurements generated by voltage ramps for the control, 5 and 10 min ABA. Inset: Superimposed I-V plots showing the average effect of ABA on  $I_{Ba}$  (0 Mg-ATP). Data are current average measurements ( $\pm$ SEM) from different experiments ( $n = 3$ ) before ( $\circ$ ) and approximately 10 min after ( $\bullet$ ) bath perfusion with ABA (Student's test; \*  $p \leq 0.05$ , \*\*  $p \leq 0.01$ , ns  $p > 0.05$ ).

After about 10 min, the time usually necessary to reach steady-state conditions, we switched the perfusion solution to the one containing  $20 \mu\text{M}$  ABA. A rapid and pronounced increase of  $I_{Ba}$  currents is seen at all voltages between  $-100$  and  $-200$  mV ( $\geq 1.3$ - to 1.5-fold) after only 5 min of ABA treatment

(Figure 5B), and a near doubling of the size of the  $I_{Ba}$  currents occurs at 10 min (Figure 5A,B). The enhancement of  $I_{Ba}$  in response to ABA, especially at 10 min, spans from  $-60$  to  $-200$  mV, and also appears to shift the activation threshold of  $I_{Ba}$  (Figure 5B) to the right. This suggests that ABA not only enhances calcium entry through HACCs but can also mobilize calcium entry at less negative voltages.

### 3.6. Characterization of the Effect of $Mg^{2+}$ on $I_{Ba}$ and $I_{K,in}$

To answer whether internal  $Mg^{2+}$  alone causes the block of  $I_{Ba}$  when we add Mg-ATP, GCPs were patched either without Mg-ATP or without ATP, but with added  $Mg^{2+}$  (added as  $MgCl_2$ ) (Figure 6).

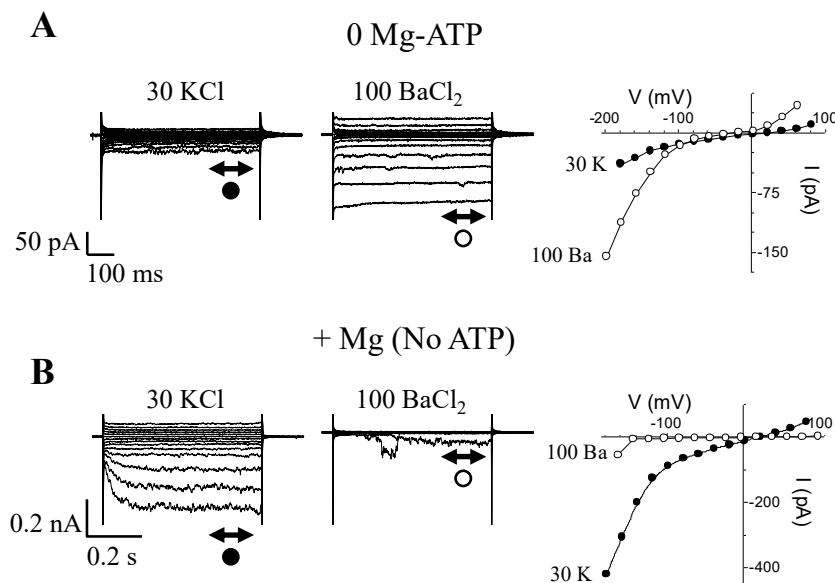


**Figure 6.** Internal  $Mg^{2+}$  is responsible for  $I_{Ba}$  inhibition. (A) Currents (left panel) and corresponding I-V plots (right panel) from the same guard cell recorded in response to hyperpolarizing voltage steps (from  $+64$  to  $-196$  mV; in  $-20$  mV increments;  $h_v = -36$  mV) and in the absence of Mg-ATP using either  $K^+$  (30 mM) or  $Ba^{2+}$  (100 mM) as charge carriers. Notice the larger  $I_{Ba}$  compared to  $I_{K,in}$ . (B) Current (left panel) and corresponding I-V relationships (right panel) recorded in the same external conditions as in (A), but this time using only  $Mg^{2+}$  ions in the patch solution (1 mM added as  $MgCl_2$ ) and no added ATP. In these conditions, the predominant current activated by hyperpolarization is  $I_{K,in}$ , not  $I_{Ba}$ .

Furthermore, and as a control for the “ion transport functionality” of the patched GCPs, we used conditions that allow measurements of not just  $I_{Ba}$ , but also to record  $I_{K,in}$ . The experiments were started in conditions allowing to probe for  $I_{K,in}$  with KCl (30 mM) in the bath, which was then followed by replacing the KCl with a solution containing  $BaCl_2$  (100 mM). This was done first in the absence of both intracellular  $Mg^{2+}$  and ATP (Figure 6A), and then repeated on another batch of guard cells with internal medium containing 1 mM  $MgCl_2$  but no ATP (Figure 6B). Firstly, in zero Mg-ATP, the only current that activated in response to hyperpolarization was  $I_{Ba}$  (Figure 6A).  $I_{K,in}$  could not be activated. Secondly, when only  $Mg^{2+}$  was included in the pipet solution (no ATP added),  $I_{K,in}$  could then be activated in 30 mM  $K^+$ . However, when switching the bath from  $K^+$ - to  $Ba^{2+}$ -containing media,  $I_{Ba}$  currents vanished, indicating that including only  $Mg^{2+}$  in the patch pipet can cause the blockage of  $I_{Ba}$  at voltages where it is normally activated in 0 Mg-ATP.

### 3.7. Can cAMP Activate HACCs in *V. faba* Guard Cells Despite the Presence of Intracellular $Mg^{2+}$ ?

We know from our own previous work [15] that cAMP activated a  $Gd^{3+}$ -sensitive HACC in guard cells while recording in  $Mg^{2+}$ - and ATP-free media (Figure 7A). However, since we had shown that this conductance discriminates poorly between divalent and monovalent cations, a hallmark characteristic of all animal and plant cyclic nucleotide gated channels (CNGCs) [13,45], we sought to check if the

$Gd^{3+}$ -sensitive  $I_{Ba}$  is also gated by cAMP in conditions where intracellular  $Mg^{2+}$  is present and  $I_{Ba}$  is already blocked (Figure 7B).

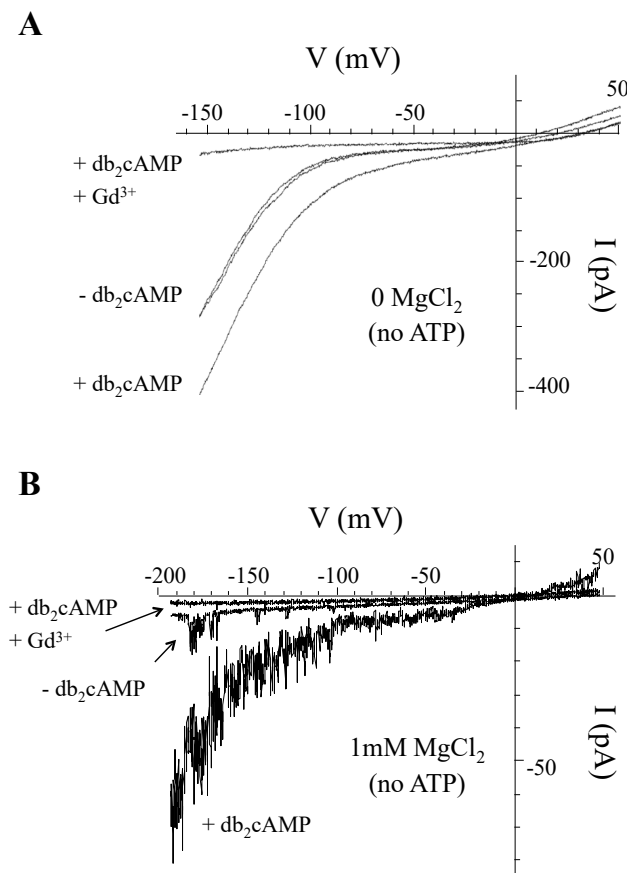


**Figure 7.** Dibutyryl 3',5'-cyclic adenosine monophosphate (cAMP) potentiates a  $Gd^{3+}$ -sensitive current in guard cells either in the presence or absence of intracellular  $Mg^{2+}$ . Experiments were conducted in the whole cell configuration, where the GCPs were held at  $-52$  mV and the I-V plots were generated using a hyperpolarizing ramp protocol. See Methods for bath and intracellular media. **(A)** Typical example from a *V. faba* GCP patched with no Mg-ATP in the intracellular media, showing superimposed I-V ramps from  $+50$  to  $-156$  mV ( $70$  mV·s<sup>-1</sup>) in the absence ( $-db_2cAMP$ ) or presence ( $+db_2cAMP$ ) of  $1$  mM dibutyryl cAMP. Note that adding  $0.05$  mM  $GdCl_3$  while keeping  $db_2cAMP$  in the bath blocks this conductance. **(B)** A representative example from an *A. thaliana* GCP patched with  $1$  mM  $MgCl_2$  (no added ATP) in the intracellular media, showing superimposed I-V ramps from  $\sim 50$  to  $-192$  mV ( $70$  mV·s<sup>-1</sup>) in the absence ( $-db_2cAMP$ ) or presence ( $+db_2cAMP$ ) of  $1$  mM dibutyryl cAMP. Note that adding  $0.05$  mM  $GdCl_3$  while keeping  $db_2cAMP$  in the bath also blocks this conductance.

In the absence of  $db_2cAMP$  (the lipophilic permeable analog of cAMP), and as expected only a small background  $I_{Ba}$  current is seen ( $\leq 10$  pA around  $-190$  mV). After perfusing with  $db_2cAMP$  ( $1$  mM), a substantial increase in  $I_{Ba}$  amplitude between voltages from around  $-30$  to  $-190$  mV was observed ( $>60$  pA around  $-190$  mV). Keeping  $db_2cAMP$  in the bath and adding  $Gd^{3+}$  ( $50$   $\mu$ M) resulted in a total block of the current ( $\leq 4$  pA around  $-190$  mV). This may indicate that GCPs harbor CNGCs that can be activated by cAMP despite the blocking effect by  $Mg^{2+}$ .

### 3.8. Identification of Candidate $Mg^{2+}$ -Dependent Cation Channels in *Arabidopsis thaliana*

Given the data from the physiological experiments, we undertook a search for candidate  $Mg^{2+}$ -dependent cation channels in plants (Figure 8).



identity. The obtained models clearly showed that AtCNGCs do not have a  $Mg^{2+}$  binding site corresponding to the location of  $K_{ir}2.2$  D173 inside the pore region (Figure 8A, left arrow, and Figure S2). However, a tandem glutamic acid motif that could form a possible diacidic  $Mg^{2+}$  binding site is found in most AtCNGCs located a little downstream of the pore, in the so-called C-linker disc (Figure 8). Akin to  $K_{ir}2.2$  D173 and E300/E225, this diacidic AtGNCG motif forms a positively charged opening, with distances of 7.3–8.3 Å between neighbouring charges and a diameter of ~11 Å (for  $K_{ir}2.2$  D173, these values are 7.3–7.4 Å and 10.4–11.8 Å, respectively (PDB 3jyc)). As in  $K_{ir}2.2$ , these distances between carboxyl groups are too large for direct ion coordination, suggesting that  $Mg^{2+}$  is bound through bridging water molecules [46]. Interestingly, this diacidic motif is not present in AtGNCG2, which has been shown to be an atypical family member with respect to ion selectivity [49]. The diacidic motif is also absent in HCN1, for which  $Mg^{2+}$  inward rectification has not been documented (Figure 8C).

#### 4. Discussion

In order to record ion currents (for instance  $I_{K,in}$  or  $I_{K,out}$ ) from plant cells in the “whole-cell” patch configuration, for reasons highlighted in the introduction (also see Methods section in [50]), it is standard to include ATP and  $Mg^{2+}$  in either the form of [Mg-ATP] or [MgCl<sub>2</sub> + K<sub>2</sub>-ATP]. In contrast, the composition of the internal solution used to characterize the hyperpolarization-activated Ca<sup>2+</sup> current (HACC or  $I_{Ba}$ ) is more variable, especially with regards to ATP and  $Mg^{2+}$ . For example, one can notice that ATP and  $Mg^{2+}$  are either both included [9,11,17,51,52] or completely omitted from the internal solution [10,16,53–55]. Here, we summarize the role and consequences of  $Mg^{2+}$  inclusion, either in the form of Mg-ATP or MgCl<sub>2</sub>. Incidentally, there are no data on cytosolic magnesium concentrations or the distribution of magnesium within the different cellular compartments of guard cells. However, we think it is reasonable to assume that intracellular free [Mg<sup>2+</sup>] is between 400 and 600 μM, which the total magnesium, including the complexed form, may be as high as 10 mM.

An overview of some of the pharmacological properties related to the HACC ( $I_{Ba}$ ) and  $I_{K,in}$  are presented in Figure 9.

	Activation by hyperpolarization:	Extracellular					Intracellular				
		Gd <sup>3+</sup>	Mn <sup>2+</sup>	Ba <sup>2+</sup>	Cs <sup>+</sup>	TEA <sup>+</sup>	Ca <sup>2+</sup>	Mg <sup>2+</sup>	ATP	cAMP/cGMP	
$I_{Ba}$	Yes	Yes	Yes (Véry & Davies, 2000)	No	No	No	Yes (Hamilton <i>et al.</i> , 2000)	Yes (decreases with high Mg <sup>2+</sup> )	No	Yes (cAMP potentiates; Lemtiri & Berkowitz, 2003)	
$I_{K,in}$	Yes	No	No	Yes	Yes	Yes (Blatt, 1992)	Yes (Schroeder & Hagiwara, 1989)	Yes (increases with high Mg <sup>2+</sup> )	No (can restore $I_{K,in}$ run down; Hoshi, 1995)	Yes (cGMP inhibits; Hoshi, 1995)	

**Figure 9.** Overview of the properties of the hyperpolarization-activated calcium channels (HACCs).

We report experiments designed to assess the effect of  $Mg^{2+}$  on  $I_{Ba}$  current activated by hyperpolarization in GCPs, being aware that other cell types, e.g., root cells, might indeed show different responses. We show that omitting Mg-ATP unmasked the presence of an instantaneously activating, inwardly rectifying conductance. This “newly unveiled” conductance still retains most of the biophysical and pharmacological characteristics that are hallmarks of the classical  $I_{Ca}$ -type [9,10] and CNGCs, which we referred to here as either  $I_{Ba}$  or HACCs [13,14]. Similarly to  $I_{K,in}$ , this conductance is activated by hyperpolarizing-going voltages, and shows some voltage-dependent rectification (but not as strongly as compared to  $I_{K,in}$ , for example; see Figure 4A). Additionally, typical of HACCs, we found that besides Ba<sup>2+</sup>, other divalent cations such as Ca<sup>2+</sup>, Sr<sup>2+</sup>, and Mn<sup>2+</sup> also permeate this

channel, but at a much slower rate than  $\text{Ba}^{2+}$  does, hence the smaller currents resolved even though the same amounts of divalent cations in the bath were used. More importantly, this HACC is activated by cAMP, as well as permeable to monovalent cations (see Figure S1), which are definite attributes of CNGCs. HACCs, including CNGCs, are specifically blocked by low concentrations of extracellular  $\text{Gd}^{3+}$  that are far less effective in blocking  $I_{K,\text{in}}$  (see Figure 4A). Equally important, we found that the unmasked  $I_{\text{Ba}}$  is also enhanced by  $\approx 1.3$ - to 1.5-fold in response to 5 min treatment with ABA and by up to 2-fold after 10 min. Similarly, it was shown that ABA increases a PM  $I_{\text{Ca}}$ -type whole-cell current in *Arabidopsis* guard cells by  $\approx 2$ - to 3-fold within 5 min of treatment [9]. Note that the ABA effect reported here was obtained not only in  $\text{Mg}^{2+}$ -free internal solution, but even more importantly in ATP-free internal solution, thus indicating that ATP is not as crucial for this channel as was suggested by an earlier report [56]. This is in agreement with many other reports showing that ABA can indeed increase cytosolic  $\text{Ca}^{2+}$  levels through activation of PM calcium channels via hyperpolarization in *Arabidopsis thaliana* guard cells [10,57,58]. Furthermore, ATP was neither required for cGMP- nor cAMP-activated [49,50]  $\text{Ca}^{2+}$ -permeable cation channels in many different plant cell types (mesophyll, guard cells, or pollen tubes) that also show many of the HACC characteristics. This observation is in contrast to the above-mentioned report, where ATP and subsequent protein (de)phosphorylation was described as a prerequisite for an ABA effect on calcium channels (56). This indicates that there may be more than one subtype of calcium channel co-existing in the PM or that additional modes of regulation of these  $\text{Ca}^{2+}$ -permeable channels are in operation, which might require ATP- and protein-kinase-dependent signalling [56,59].

One discrepancy that stands out in our report is that  $\text{Mg}^{2+}$  was shown to permeate HACCs in guard cells [10] and in root hairs [51], whereas in our experiments external  $\text{Mg}^{2+}$  did not appear to permeate this channel (Figure 3A). This is even more intriguing when considering that cGMP was recently shown to activate an inward rectifying current (which was also lanthanide-sensitive), with  $\text{Mg}^{2+}$  as a charge carrier [16]. Hence, this is another hint that we may be dealing with more than one subtype of calcium channel. In animal cells,  $\text{Mn}^{2+}$  was described as a blocker of calcium channels if  $\text{Ca}^{2+}$  is present in the bath, while in the absence of  $\text{Ca}^{2+}$  the  $\text{Mn}^{2+}$  permeates the channel [60,61]. These data might infer that HACCs, despite sharing many similarities in terms of their biophysical and pharmacological characteristics, might slightly differ from one cell type to another depending on the tissue type or plant species.

Therefore, the first key finding is that omitting Mg-ATP from the intracellular medium unmasks a larger  $\text{Gd}^{3+}$ -sensitive, non-selective cation conductance that is also regulated by cAMP and ABA. The mechanism consists of shifting the I-V characteristic to the right, where less negative voltages can mobilize cations (including  $\text{Ca}^{2+}$ ) through the channel. The second key finding is the demonstration that  $\text{Mg}^{2+}$  alone can block this conductance (Figure 6).

The current activated by voltages lower than  $-200$  mV is small but significant (Figure 1A). At the present time, we have no evidence to support that this instantaneous, rectifying,  $\text{Mg}^{2+}$ -resistant  $\text{Ba}^{2+}$  current would be carried by a different population type of HACCs (the channel type that was unmasked when  $\text{Mg}^{2+}$  was omitted). If anything, this current could still be carried by the same type of channel, since addition of  $20 \mu\text{M}$   $\text{Gd}^{3+}$  to the bath was still able to swiftly and efficiently block this current.

Our data describe that in guard cells,  $\text{Mg}^{2+}$  blocks  $I_{\text{Ba}}$  by shifting the I-V relationship and its activation threshold to more negative voltages (Figure 1C). This effect is reminiscent of the inhibitory effects by  $\text{Mg}^{2+}$  on many ion channels, which have been interpreted as “charge screening effects” [18]. Indeed, the rectification of the inwardly rectifying  $\text{K}^+$  ( $\text{K}_{\text{ir}}$ ) channels is due to a voltage-dependent blockage by cytosolic  $\text{Mg}^{2+}$  (and polyamines), thereby blocking outward  $\text{K}^+$ -efflux. Upon hyperpolarization,  $\text{Mg}^{2+}$  is ejected from the pore, which appears to result in a time-dependent opening of the channel [62,63]. Likewise, TRPV6 shows  $\text{Mg}^{2+}$ -dependent gating that contributes to its strong inward rectification [20]; it was suggested that  $\text{Mg}^{2+}$  can block the channel by binding to a site within the transmembrane electrical field, where it interacts with other permeant cations [20]. It is also

conceivable that other mechanisms could be operating, such as electrostatic interaction between  $Mg^{2+}$  and some PM lipids, such as phosphatidylinositol 4,5-bisphosphate (or  $PIP_2$ ). It was demonstrated that increasing the amount of membrane  $PIP_2$  results in decreasing the sensitivity of KCNQ channel to inhibition by  $Mg^{2+}$  [64]. In addition, some  $Ca^{2+}$  channels were found to require  $PIP_2$  for their normal function [65]. This begs the question of whether guard cell PM  $Ca^{2+}$  channels are also  $PIP_2$ -sensitive. Our results also raise the question of whether  $Mg^{2+}$  could be equally important for  $I_{K,in}$  gating. Indeed, unlike earlier reports, we found that activation of  $I_{K,in}$  was dependent on  $Mg^{2+}$  being present inside the patch pipet (Figure 6).

Furthermore, the activation of the above HACCs by hyperpolarization and cAMP, the absence of cation selectivity, and inhibition by lanthanides is consistent with the hypothesis that channels responsible for the observed effects are CNGCs. This is consistent with our structural modelling, which revealed the presence of diacidic motifs in the pore-forming helix of a subset of AtCNGCs. Acidic residues pointing towards the inner side of the pore, have previously been shown to confer  $Mg^{2+}$  dependence to inward rectifying  $K^+$  channels in animals [47] (Figure S2B). Given the position of the diacidic motif in the cytoplasmic side of the pore, it is conceivable that  $Mg^{2+}$  binding can be affected by changes in pore opening, for example introduced by cAMP binding to the cytoplasmic region of AtCNGCs. Such crosstalk would provide a mechanistic explanation for our observation that cAMP overrides the channel blockage produced by 1mM  $MgCl_2$  (no added ATP) (Figure S2C), thereby preventing uncontrolled  $Ca^{2+}$  leakage.

## 5. Conclusions

Here, we firstly propose that in *Vicia faba* guard cells,  $Mg^{2+}$  can limit or prevent continuous  $Ca^{2+}$ -leakage, possibly through all HACCs (including CNGCs) at resting membrane potentials, thereby being part of the (intra)cellular calcium signaling processes [66]. Furthermore, CNGCs have also been recognized as having a critical role in  $Ca^{2+}$ -dependent plant defense signalling and responses [67,68]. Secondly, we propose that the activation of these channels requires mechanism(s) by which  $Mg^{2+}$  binding is altered. In CNGCs, such a mechanism is conceivably enabled by cAMP binding, thereby assigning  $Mg^{2+}$  an important role in calcium homeostasis and calcium-dependent downstream processes. Finally, the effect reported here suggests that  $Mg^{2+}$  has a role in cellular  $Ca^{2+}$  homeostasis, similarly to in animal cells.

**Supplementary Materials:** Supplementary materials can be found at <http://www.mdpi.com/1422-0067/21/11/3771/s1>: Supplementary Figure S1: In the absence of MgATP, guard cell HACCs are permeable to monovalent cations, such as  $K^+$ ,  $Na^+$ , and  $Cs^+$ , but not  $TEA^+$ . All experiments were conducted in the whole cell configuration, where *V. faba* GCPs were held at  $-56$  mV. (A) Superimposed I-V plots in the presence of 100 mM  $BaCl_2$  (■), 100 mM KCl (▲), or 100 mM KCl + 0.05 mM  $GdCl_3$ . (B) Superimposed I-V plots in the presence of 100 mM  $BaCl_2$  (■), 100 mM NaCl (□), or 100 mM NaCl + 0.05 mM  $GdCl_3$ . (C) Superimposed I-V plots in the presence of 100 mM  $BaCl_2$  (■) or 100 mM  $CsCl$  (□), or 100 mM  $CsCl$  + 0.05 mM  $GdCl_3$  (◻). (D) Superimposed I-V plots in the presence of 100 mM  $BaCl_2$  (■) or 100 mM TEACl (▼). Supplementary Figure S2: (A) Alignment of the *Arabidopsis thaliana* CNGC8 pore region and the Kir2.2 (PDB accession number 5u6o\_341\_471). (B) Mechanism of inward rectification by magnesium ions. Tao et al. (Science 2009, 326, 1668-1674) have shown that inward rectification through  $Mg^{2+}$  can be explained by the ion binding to negatively charged regions in the pore (formed by D173) and in the cytoplasmic regulatory domains (D256 and E300/E225). The crystal structure of the inward rectifying potassium channel Kir2.2 (Tao, 2009; PDB entry 3JYC) is shown in ribbon presentation. The four subunits are color-coded. Potassium ions in the channel are shown as magenta spheres. Negatively charged residues that bind the  $Mg^{2+}$  mimic  $Sr^{2+}$  in the crystal structure are shown in pink on their molecular surfaces. (C) Sequences of pore-forming transmembrane helix (TM) from AtCNGCs. The TM is marked with a dashed line. Models were built using Swiss-Model (Waterhouse et al. (Nucleic Acids Res. 2018, 46, W296-W303)).

**Author Contributions:** F.L.-C. and C.G. conceived the study. F.L.-C. performed the experiments and analyzed the data. C.G. and S.T.A. performed the structural analyses. All authors have read and agreed to the published version of the manuscript.

**Funding:** This research has been supported by the King Abdullah University of Science and Technology (KAUST). We are indebted to Enid MacRobbie (Department of Plant Science, University of Cambridge, UK) for allowing us to use some of the data gathered by F.L.-C. whilst in her laboratory (research was supported by BBSRC Grant P05730 to E.M.). We also thank Mark Tester for his invaluable comments.

**Acknowledgments:** We also thank Mark Tester for his invaluable comments.

**Conflicts of Interest:** The authors declare no conflict of interest.

## References

1. McAinsh, M.R.; Pittman, J.K. Shaping the calcium signature. *New Phytol.* **2009**, *181*, 275–294. [[CrossRef](#)] [[PubMed](#)]
2. Véry, A.A.; Sentenac, H. Cation channels in the *Arabidopsis* plasma membrane. *Trends Plant Sci.* **2002**, *7*, 168–175. [[CrossRef](#)]
3. White, P.J.; Broadley, M.R. Calcium in plants. *Ann. Bot.* **2003**, *92*, 487–511. [[CrossRef](#)] [[PubMed](#)]
4. Demidchik, V.; Davenport, R.J.; Tester, M. Nonselective cation channels in plants. *Annu. Rev. Plant Biol.* **2002**, *53*, 67–107. [[CrossRef](#)]
5. Thion, L.; Mazars, C.; Nacry, P.; Bouchez, D.; Moreau, M.; Ranjeva, R.; Thuleau, P. Plasma membrane depolarization-activated calcium channels, stimulated by microtubule-depolymerizing drugs in wild-type *Arabidopsis thaliana* protoplasts, display constitutively large activities and a longer half-life in *ton 2* mutant cells affected in the organization of cortical microtubules. *Plant J.* **1998**, *13*, 603–610.
6. Miedema, H.; Bothwell, J.H.; Brownlee, C.; Davies, J.M. Calcium uptake by plant cells - channels and pumps acting in concert. *Trends Plant Sci.* **2001**, *6*, 514–519. [[CrossRef](#)]
7. MacRobbie, E.A.C. Calcium and ABA-induced stomatal closure. *Philos. Trans. Roy. Soc. B.* **1992**, *338*, 5–18.
8. MacRobbie, E.A.C. ABA activates multiple  $\text{Ca}^{2+}$  fluxes in stomatal guard cells, triggering vacuolar  $\text{K}^+$  ( $\text{Rb}^+$ ) release. *Proc. Natl. Acad. Sci. USA* **2000**, *97*, 12361–12368. [[CrossRef](#)]
9. Hamilton, D.W.A.; Hills, A.; Köhler, B.; Blatt, M.R.  $\text{Ca}^{2+}$  channels at the plasma membrane of stomatal guard cells are activated by hyperpolarization and abscisic acid. *Proc. Natl. Acad. Sci. USA* **2000**, *97*, 4967–4972. [[CrossRef](#)]
10. Pei, Z.M.; Murata, Y.; Benning, G.; Thomine, S.; Klusener, B.; Allen, G.J.; Grill, E.; Schroeder, J.I. Calcium channels activated by hydrogen peroxide mediate abscisic acid signalling in guard cells. *Nature* **2000**, *406*, 731–734. [[CrossRef](#)]
11. Hamilton, D.W.A.; Hills, A.; Blatt, M.R. Extracellular  $\text{Ba}^{2+}$  and voltage interact to gate  $\text{Ca}^{2+}$  channels at the plasma membrane of stomatal guard cells. *FEBS Lett.* **2001**, *491*, 99–103. [[CrossRef](#)]
12. Leng, Q.; Mercier, R.W.; Yao, W.; Berkowitz, G.A. Cloning and first functional characterization of a plant cyclic nucleotide-gated cation channel. *Plant Physiol.* **1999**, *121*, 753–761. [[CrossRef](#)] [[PubMed](#)]
13. Leng, Q.; Mercier, R.W.; Hua, B.G.; Fromm, H.; Berkowitz, G.A. Electrophysiological analysis of cloned cyclic nucleotide-gated ion channels. *Plant Physiol.* **2002**, *128*, 400–410. [[CrossRef](#)] [[PubMed](#)]
14. Balagué, C.; Lin, B.Q.; Alcon, C.; Flottes, G.; Malmström, S.; Köhler, C.; Neuhaus, G.; Pelletier, G.; Gaymard, F.; Roby, D. HLM1, an essential signaling component in the hypersensitive response, is a member of the cyclic nucleotide-gated channel ion channel family. *Plant Cell* **2003**, *15*, 365–379. [[CrossRef](#)] [[PubMed](#)]
15. Lemtiri-Chlieh, F.; Berkowitz, G.A. Cyclic adenosine monophosphate regulates calcium channels in the plasma membrane of *Arabidopsis* leaf guard and mesophyll cells. *J. Biol. Chem.* **2004**, *279*, 35306–35312. [[CrossRef](#)] [[PubMed](#)]
16. Wang, Y.F.; Munemasa, S.; Nishimura, N.; Ren, H.M.; Robert, N.; Han, M.; Puzorjova, I.; Kollist, H.; Lee, S.; Mori, I.; et al. Identification of cyclic GMP-activated nonselective  $\text{Ca}^{2+}$ -permeable cation channels and associated CNGC5 and CNGC6 genes in *Arabidopsis* guard cells. *Plant Physiol.* **2013**, *163*, 578–590. [[CrossRef](#)]
17. Wu, J.Y.; Qu, H.Y.; Jin, C.; Shang, Z.L.; Wu, J.; Xu, G.H.; Gao, Y.B.; Zhang, S.L. cAMP activates hyperpolarization-activated  $\text{Ca}^{2+}$ -channels in the pollen of *Pyrus pyrifolia*. *Plant Cell Rep.* **2011**, *30*, 1193–1200. [[CrossRef](#)] [[PubMed](#)]
18. Hille, B. *Ion Channels of Excitable Membranes*, 3rd ed.; Sinauer Associates, Inc.: Sunderland, MA, USA, 2001.
19. Matsuda, H. Open-state substructure of inwardly rectifying potassium channels revealed by magnesium block in guinea-pig heart-cells. *J. Physiol.* **1988**, *397*, 237–25820. [[CrossRef](#)]
20. Voets, T.; Janssens, A.; Prenen, J.; Droogmans, G.; Nilius, B.  $\text{Mg}^{2+}$ -dependent gating and strong inward rectification of the cation channel TRPV6. *J. Gen. Physiol.* **2003**, *121*, 245–260. [[CrossRef](#)]
21. Zito, K.; Scheuss, V. NMDA Receptor Function and Physiological Modulation. In *Encyclopedia of Neuroscience*; Squire, L.R., Ed.; Academic Press: Oxford, UK, 2009.



22. Nowak, L.M.; Ascher, P.; Bregestovski, P.; Herbet, A.; Prochiantz, A. Voltage dependence of 1-Glu induced current is due to gating by Mg ions. *Biophys. J.* **1984**, *45*, A388.
23. Schroeder, J.I. Magnesium-independent activation of inward-rectifying K<sup>+</sup> channels in *Vicia-faba* guard-cells. *FEBS Lett.* **1995**, *363*, 157–160. [[CrossRef](#)]
24. Hedrich, R.; Moran, O.; Conti, F.; Busch, H.; Becker, D.; Gambale, F.; Dreyer, I.; Kuch, A.; Neuwinger, K.; Palme, K. Inward rectifier potassium channels in plants differ from their animal counterparts in response to voltage and channel modulators. *Eur. Biophys. J.* **1995**, *24*, 107–115. [[CrossRef](#)]
25. Pei, Z.M.; Ward, J.M.; Schroeder, J.I. Magnesium sensitizes slow vacuolar channels to physiological cytosolic calcium and inhibits fast vacuolar channels in fava bean guard cell vacuoles. *Plant Physiol.* **1999**, *121*, 977–986. [[CrossRef](#)]
26. Brüggemann, L.I.; Pottosin, I.I.; Schönknecht, G. Cytoplasmic magnesium regulates the fast activating vacuolar cation channel. *J. Exp. Bot.* **1999**, *50*, 1547–1552. [[CrossRef](#)]
27. Carpaneto, A.; Cantu, A.M.; Gambale, F. Effects of cytoplasmic Mg<sup>2+</sup> on slowly activating channels in isolated vacuoles of *Beta vulgaris*. *Planta* **2001**, *213*, 457–468. [[CrossRef](#)] [[PubMed](#)]
28. Pottosin, I.; Martinez-Estevéz, M.; Dobrovinskaya, O.; Muniz, J.; Schönknecht, G. Mechanism of luminal Ca<sup>2+</sup> and Mg<sup>2+</sup> action on the vacuolar slowly activating channels. *Planta* **2004**, *219*, 1057–1070. [[CrossRef](#)] [[PubMed](#)]
29. Wolf, T.; Guinot, D.R.; Hedrich, R.; Dietrich, P.; Marten, I. Nucleotides and Mg<sup>2+</sup> ions differentially regulate K<sup>+</sup> channels and non-selective cation channels present in cells forming the stomatal complex. *Plant Cell Physiol.* **2005**, *46*, 1682–1689. [[CrossRef](#)]
30. Tyerman, S.D.; Whitehead, L.F.; Day, D.A. A channel-like transporter for NH<sub>4</sub><sup>+</sup> on the symbiotic interface of N<sub>2</sub>-fixing plants. *Nature* **1995**, *378*, 629–632. [[CrossRef](#)]
31. Obermeyer, G.; Tyerman, S.D. NH<sub>4</sub><sup>+</sup> currents across the peribacteroid membrane of soybean. Macroscopic and microscopic properties, inhibition by Mg<sup>2+</sup>, and temperature dependence indicate a subpicosiemens channel finely regulated by divalent cations. *Plant Physiol.* **2005**, *139*, 1015–1029. [[CrossRef](#)]
32. Babenko, A.P.; Aguilar-Bryan, L.; Bryan, J. A view of SUR/K<sub>IR</sub>6.X, K<sub>ATP</sub> channels. *Annu. Rev. Physiol.* **1998**, *60*, 667–687. [[CrossRef](#)]
33. Campbell, J.D.; Sansom, M.S.P.; Ashcroft, F.M. Potassium channel regulation - Structural insights into the function of the nucleotide-binding domains of the human sulphonylurea receptor. *EMBO Rep.* **2003**, *4*, 1038–1042. [[CrossRef](#)] [[PubMed](#)]
34. Assmann, S.M.; Simoncini, L.; Schroeder, J.I. Blue-light activates electrogenic ion pumping in guard-cell protoplasts of *Vicia faba*. *Nature* **1985**, *318*, 285–287. [[CrossRef](#)]
35. Schroeder, J.I. K<sup>+</sup> Transport-properties of K<sup>+</sup> channels in the plasma-membrane of *Vicia faba* guard-cells. *J. Gen. Physiol.* **1988**, *92*, 667–683. [[CrossRef](#)]
36. Blatt, M.R. Electrical characteristics of stomatal guard-cells—The ionic basis of the membrane-potential and the consequence of KCl leakage from microelectrodes. *Planta* **1987**, *170*, 272–287. [[CrossRef](#)] [[PubMed](#)]
37. Lemtiri-Chlieh, F. Effects of internal K<sup>+</sup> and ABA on the voltage- and time-dependence of the outward K<sup>+</sup>-rectifier in *Vicia* guard cells. *J. Memb. Biol.* **1996**, *153*, 105–116. [[CrossRef](#)] [[PubMed](#)]
38. Lemtiri-Chlieh, F.; Macrobbe, E.A.C. Role of calcium in the modulation of *Vicia* guard-cell potassium channels by abscisic acid: A patch-clamp study. *J. Memb. Biol.* **1994**, *137*, 99–107. [[CrossRef](#)]
39. Neher, E. Correction for liquid junction potentials in patch clamp experiments. *Methods Enzymol.* **1992**, *207*, 123–131.
40. Shaff, J.E.; Schultz, B.A.; Craft, E.J.; Clark, R.T.; Kochian, L.V. GEOCHEM-EZ: A chemical speciation program with greater power and flexibility. *Plant Soil* **2010**, *330*, 207–214. [[CrossRef](#)]
41. Waterhouse, A.; Bertoni, M.; Bienert, S.; Studer, G.; Tauriello, G.; Gumienny, R.; Heer, F.T.; de Beer, T.A.P.; Rempfer, C.; Bordoli, L.; et al. SWISS-Model: Homology modelling of protein structures and complexes. *Nucleic Acids Res.* **2018**, *46*, W296–W303. [[CrossRef](#)]
42. Buchan, D.W.; Minnici, F.; Nugent, T.C.; Bryson, K.; Jones, D.T. Scalable web services for the PSIPRED Protein Analysis Workbench. *Nucleic Acids Res.* **2013**, *41*, W349–W357. [[CrossRef](#)] [[PubMed](#)]
43. Edgar, R.C. MUSCLE: A multiple sequence alignment method with reduced time and space complexity. *BMC Bioinform.* **2004**, *5*, 113. [[CrossRef](#)]
44. Blatt, M.R. K<sup>+</sup> channels of stomatal guard-cells—Characteristics of the inward rectifier and its control by pH. *J. Gen. Physiol.* **1992**, *99*, 615–644. [[CrossRef](#)] [[PubMed](#)]

45. Zagotta, W.N.; Siegelbaum, S.A. Structure and function of cyclic nucleotide-gated channels. *Ann. Rev. Neurosci.* **1996**, *19*, 235–263. [[CrossRef](#)]
46. Tao, X.; Avalos, J.L.; Chen, J.; MacKinnon, R. Crystal structure of the eukaryotic strong inward-rectifier K<sup>+</sup> channel K<sub>ir</sub>2.2 at 3.1 Å resolution. *Science* **2009**, *326*, 1668–1674. [[CrossRef](#)] [[PubMed](#)]
47. Zelman, A.K.; Dawe, A.; Gehring, C.; Berkowitz, G.A. Evolutionary and structural perspectives of plant cyclic nucleotide-gated cation channels. *Front. Plant Sci.* **2012**, *3*, 95. [[CrossRef](#)] [[PubMed](#)]
48. Clayton, G.M.; Altieri, S.; Heginbotham, L.; Unger, V.M.; Morais-Cabral, J.H. Structure of the transmembrane regions of a bacterial cyclic nucleotide-regulated channel. *Proc. Natl. Acad. Sci. USA* **2008**, *105*, 1511–1515. [[CrossRef](#)] [[PubMed](#)]
49. Hua, B.G.; Mercier, R.W.; Leng, Q.; Berkowitz, G.A. Plants do it differently. A new basis for potassium/sodium selectivity in the pore of an ion channel. *Plant Physiol.* **2003**, *132*, 1353–1361. [[CrossRef](#)]
50. Bush, D.S.; Hedrich, R.; Schroeder, J.I.; Jones, R.L. Channel-mediated K<sup>+</sup> flux in barley aleurone protoplasts. *Planta* **1988**, *176*, 368–377. [[CrossRef](#)]
51. Véry, A.A.; Davies, J.M. Hyperpolarization-activated calcium channels at the tip of *Arabidopsis* root hairs. *Proc. Natl. Acad. Sci. USA* **2000**, *97*, 9801–9806. [[CrossRef](#)] [[PubMed](#)]
52. Miedema, H.; Demidchik, V.; Véry, A.A.; Bothwell, J.H.F.; Brownlee, C.; Davies, J.M. Two voltage-dependent calcium channels co-exist in the apical plasma membrane of *Arabidopsis thaliana* root hairs. *New Phytol.* **2008**, *179*, 378–385. [[CrossRef](#)]
53. Murata, Y.; Pei, Z.M.; Mori, I.C.; Schroeder, J. Abscisic acid activation of plasma membrane Ca<sup>2+</sup> channels in guard cells requires cytosolic NAD(P)H and is differentially disrupted upstream and downstream of reactive oxygen species production in *abi1-1* and *abi2-1* protein phosphatase 2C mutants. *Plant Cell* **2001**, *13*, 2513–2523. [[CrossRef](#)] [[PubMed](#)]
54. Demidchik, V.; Bowen, H.C.; Maathuis, F.J.M.; Shabala, S.N.; Tester, M.A.; White, P.J.; Davies, J.M. *Arabidopsis thaliana* root non-selective cation channels mediate calcium uptake and are involved in growth. *Plant J.* **2002**, *32*, 799–808. [[CrossRef](#)] [[PubMed](#)]
55. Lemtiri-Chlieh, F.; MacRobbie, E.A.C.; Webb, A.A.R.; Manison, N.F.; Brownlee, C.; Skepper, J.N.; Chen, J.; Prestwich, G.D.; Brearley, C.A. Inositol hexakisphosphate mobilizes an endomembrane store of calcium in guard cells. *Proc. Natl. Acad. Sci. USA* **2003**, *100*, 10091–10095. [[CrossRef](#)] [[PubMed](#)]
56. Köhler, B.; Blatt, M.R. Protein phosphorylation activates the guard cell Ca<sup>2+</sup> channel and is a prerequisite for gating by abscisic acid. *Plant J.* **2002**, *32*, 185–194. [[CrossRef](#)] [[PubMed](#)]
57. Munemasa, S.; Oda, K.; Watanabe-Sugimoto, M.; Nakamura, Y.; Shimoishi, Y.; Murata, Y. The coronatine-insensitive 1 mutation reveals the hormonal signaling interaction between abscisic acid and methyl jasmonate in *Arabidopsis* guard cells. Specific impairment of ion channel activation and second messenger production. *Plant Physiol.* **2007**, *143*, 1398–1407. [[CrossRef](#)]
58. Vahisalu, T.; Kollist, H.; Wang, Y.F.; Nishimura, N.; Chan, W.Y.; Valerio, G.; Lamminmäki, A.; Brosche, M.; Moldau, H.; Desikan, R.; et al. SLAC1 is required for plant guard cell S-type anion channel function in stomatal signalling. *Nature* **2008**, *452*, 487–491. [[CrossRef](#)]
59. Mori, I.C.; Murata, Y.; Yang, Y.; Munemasa, S.; Wang, Y.F.; Andreoli, S.; Tiriack, H.; Alonso, J.M.; Harper, J.F.; Ecker, J.R.; et al. CDPKs CPK6 and CPK3 function in ABA regulation of guard cell S-type anion- and Ca<sup>2+</sup>-permeable channels and stomatal closure. *PLoS Biol.* **2006**, *4*, e327. [[CrossRef](#)]
60. Coraboeuf, E. Voltage clamp studies of the slow inward current. In *The Slow Inward Current and Cardiac Arrhythmias*, 1st ed.; Martinus Nijhoff: The Hague, The Netherlands, 1980; pp. 25–95.
61. Bannister, R.A.; Pessah, I.N.; Beam, K.G. The skeletal L-type Ca<sup>2+</sup> current is a major contributor to excitation-coupled Ca<sup>2+</sup> entry. *J. Gen. Physiol.* **2009**, *133*, 79–91. [[CrossRef](#)]
62. Nichols, C.G.; Lopatin, A.N. Inward rectifier potassium channels. *Annu. Rev. Physiol.* **1997**, *59*, 171–191. [[CrossRef](#)]
63. Guo, D.L.; Ramu, Y.; Klem, A.M.; Lu, Z. Mechanism of rectification in inward-rectifier K<sup>+</sup> channels. *J. Gen. Physiol.* **2003**, *121*, 261–275. [[CrossRef](#)] [[PubMed](#)]
64. Suh, B.C.; Hille, B. Electrostatic interaction of internal Mg<sup>2+</sup> with membrane PIP<sub>2</sub> seen with KCNQ K<sup>+</sup> channels. *J. Gen. Physiol.* **2007**, *130*, 241–256. [[CrossRef](#)]
65. Gamper, N.; Reznikov, V.; Yamada, Y.; Yang, J.; Shapiro, M.S. Phosphatidylinositol 4,5-bisphosphate signals underlie receptor-specific G<sub>q/11</sub>-mediated modulation of N-type Ca<sup>2+</sup> channels. *J. Neurosci.* **2004**, *24*, 10980–10992. [[CrossRef](#)] [[PubMed](#)]

66. Stael, S.; Wurzinger, B.; Mair, A.; Mehlmer, N.; Vothknecht, U.C.; Teige, M. Plant organellar calcium signalling: An emerging field. *J. Exp. Bot.* **2012**, *63*, 1525–1542. [[CrossRef](#)] [[PubMed](#)]
67. Ali, R.; Ma, W.; Lemtiri-Chlieh, F.; Tsaltas, D.; Leng, Q.; von Bodman, S.; Berkowitz, G.A. Death don't have no mercy and neither does calcium: Arabidopsis CYCLIC NUCLEOTIDE GATED CHANNEL2 and innate immunity. *Plant Cell* **2007**, *19*, 181–195. [[CrossRef](#)]
68. Meena, M.K.; Prajapati, R.; Krishna, D.; Divakaran, K.; Pandey, Y.; Reichelt, M.; Mathew, M.K.; Boland, W.; Mithöfer, A.; Vadassery, J. The Ca<sup>2+</sup> channel CNGC19 regulates Arabidopsis defense against Spodoptera herbivory. *Plant Cell* **2019**, *31*, 1539–1562. [[CrossRef](#)]



© 2020 by the authors. Licensee MDPI, Basel, Switzerland. This article is an open access article distributed under the terms and conditions of the Creative Commons Attribution (CC BY) license (<http://creativecommons.org/licenses/by/4.0/>).